SCIENCE CHINA
Technological Sciences

•Article•

https://doi.org/10.1007/s11431-022-2143-6

First results of the low energy ion spectrometer onboard a Chinese geosynchronous satellite

SHAN Xu[1†*], MIAO Bin[2†], CAO Zhe[3], SUN ZhenYu[3], LI YiRen[2], LIU Kai[2], GUO XingYu[1], QU SanBiao[1], SU ZhenPeng[2], SHEN ChengLong[2], PAN ZongHao[2], LI Xin[2], HAO XinJun[2], YANG XiaoPing[4], TIAN Chao[5], JIANG Yu[5], LIU ShuBin[3], AN Qi[3], CHEN XiangJun[1] & WANG YuMing[2,6*]

[1] *Hefei National Research Center for Physical Sciences at the Microscale, Department of Modern Physics, University of Science and Technology of China, Hefei 230026, China;*
[2] *CAS Key Laboratory of Geospace Environment, School of Earth and Space Sciences, University of Science and Technology of China, Hefei 230026, China;*
[3] *State Key Laboratory of Particle Detection and Electronics (IHEP-USTC), Department of Modern Physics, University of Science and Technology of China, Hefei 230026, China;*
[4] *Shandong Institute of Space Electronic Technology, Yantai 264003, China;*
[5] *State Key Laboratory of Astronautic Dynamics, Xi'an Satellite Control Center, Xi'an 710043, China;*
[6] *CAS Center for Excellence in Comparative Planetology, University of Science and Technology of China, Hefei 230026, China*

Received May 18, 2022; accepted July 6, 2022; published online March 22, 2023

A Chinese geosynchronous satellite was launched on June 23, 2020. It carried a plasma detection package to monitor the space environment around the orbit. Here we report the inflight performance of a low energy ion spectrometer (LEIS), one of the primary instruments in the plasma detection package, and its initial observations in flight. Benefiting from the state-of-the-art design of a top-hat electrostatic analyzer cooperated with angular scanning deflectors, three-dimensional measurement of ions in space with a large field of view of 360°×90° and a wide energy range from 50 eV to 25 keV per charge has been achieved. The differential energy flux spectra of ions around the orbit have shown clear signatures of surface charging and storm/substorm ion injections. The occurrence of surface charging could be caused by the lack of photoemission at the Earth's eclipse (near the midnight) or the storm energetic electron injection at the dawn sector. The present results demonstrated a good performance of the LEIS payload in flight for monitoring the space ion environment around the orbit. *In situ* measurements of the LEIS payload provide us an opportunity to understand the magnetospheric ion dynamics and forecast the associate space weather impacts.

low energy ion spectrometer, geosynchronous orbit, inflight measurement, differential energy flux, surface charging, storm/substorm

Citation: Shan X, Miao B, Cao Z, et al. First results of the low energy ion spectrometer onboard a Chinese geosynchronous satellite. Sci China Tech Sci, 2023, 66, https://doi.org/10.1007/s11431-022-2143-6

1 Introduction

The space around Earth (geospace) has been used by multifarious satellites for various purposes such as communications, Earth observation, positioning, and navigation. Operation safety is fundamental to the satellite industry. This safety issue is deeply affected by space weather [1–3]. The Sun's activity produces a widely dynamic and significant variation of space weather, including plasma and geo-

†These authors contributed equally to this work.
*Corresponding authors (email: xshan@ustc.edu.cn; ymwang@ustc.edu.cn)

magnetism fluctuations. The geospace plasma disturbances driven by solar wind-magnetosphere interactions are one of the major sources of satellite anomaly. Among them, the charging/discharging events are recognized as a critical threat factor, closely related to malfunction and anormal scenes of satellite electronics [3–7]. There are two types of charging mechanism that will cause discharging, namely, internal (deep) charging and surface charging. The internal charging occurs inside the satellite structure and is produced by the penetrating of high-energy particles with energies higher than several hundred keV for electrons and several MeV for ions. Surface charging occurs on the surface of the satellite structure and is caused by exposure to low-energy plasma with energies from several tens to several hundred keV. An electric potential is formed on the surface of the satellite by the inflow of ions and electrons from the plasma environment around the satellite and the emission of photoelectrons because of sunlight. It is obvious that the plasma itself is a trigger leading to the charging/discharging events. *In situ* measurement of plasma in space is the most direct and significant way to grasp the plasma and its variations which can serve as the space weather monitoring and early warning. Furthermore, from the view of point of scientific research, the measured plasma fluxes, especially for the time-resolved three-dimensional (3D) distribution functions, are essential for a comprehensive understanding of plasma processes, behaviors, and interactions with others. In the past decades, various plasma detection instruments have been rapidly developed and widely used in many missions for space weather monitoring or scientific studies [8–25].

The Chinese geosynchronous satellite is close to the coordinates (R=42158 km, Azimuthal=110.5°, Co-Latitude =88.7°) and the magnetic longitude of about −177°. A low energy ion spectrometer (LEIS) onboard the satellite is one of the primary instruments in the plasma detection package for monitoring the space environment around the orbit. The LEIS payload inherited our previous instrument for the SJ18 mission [25], utilizing a cooperative configuration of angular scanning deflectors and the top-hat electrostatic spherical analyzer (ESA) to achieve a 360°×90° large field of view (FOV). It possesses the capability of detecting three-dimensional energetic ion distributions with a wide energy range of up to 25 keV/q, as well as good spatial and temporal resolutions. The main purpose of the LEIS is to sample the ion flux in 3D space, and monitor possible surface charging and magnetospheric storm or substorm events.

In this article, we focused on the inflight performance and initial observations of the LEIS payload. Measurement of energetic ions from 50 eV to 25 keV per charge in the 360°×90° FOV has been fulfilled. The initial data acquired via sixteen channels for 0°–360° azimuthal angles and −45°–+45° elevation angles have been processed to obtain reliable data for pure ions by removing the background noise and solar ultraviolet (UV) light response. The obtained ion fluxes are comparable to previous measurements by the Van Allen Probes mission near the geosynchronous orbit (GEO). The differential energy flux spectra of ions clearly demonstrate the surface charging and magnetospheric storm/substorm injection signatures.

2 Description of spectrometer and inflight measurement

The LEIS spectrometer is an update of our heritage instrument for the SJ18 mission [25], persisting an advanced design of the top-hat ESA combined with angular scanning deflectors to achieve a large FOV coverage of 360° azimuthal angles and 90° elevation angles, but the measured ion energy range is extended significantly from 50 eV/q up to 25 keV/q. By using the ways such as the simulations via Simion software and calibration experiments via a low-energy ion source in the laboratory, which are introduced detailedly in our previous work [25], the key parameters of the present spectrometer are obtained, as listed in Table 1. The improvement in its capability, compared with our previous version, is noticeable.

Figure 1(a) presents the structural and functional schematic diagram of the LEIS spectrometer. It mainly consists of a pair of angular scanning deflectors, a top-hat ESA with a position-sensitive detector, and an electronic system. The top-hat ESA has an inner sphere (with radius R_1=36 mm), an outer sphere (with radius R_2=38 mm), and a small "top-hat" section (with radius R_3=40 mm). The position sensitive detector (PSD) is composed of a pair of annular microchannel plates (MCPs) and 16 discrete anodes. As the spectrometer works, the elevation angles of ions from −45° to +45° are determined by scanning the deflector voltages (U_{def1} and U_{def2}). The ion energies are analyzed by sweeping ESA voltages (U_{inner}). The azimuth angles of ions are divided into 16 independent sections (each 22.5°) by 16 discrete anodes, signed as 16 channels from Ch1 to Ch16 as shown in Figure 1(c).

The electronic system includes a digital processing unit (DPU) board, a high voltage (HV) power supply board, and a secondary power supply board. Analog signals output from 16 discrete anodes are swiftly amplified and transferred into digital signals by 16 independent low-noise charge-sensitive amplifiers/discriminators (A121). The threshold of each A121 chip for the input signal can be adjusted remotely through the designed reference voltage. The radiation-hardened DPU is developed on the basis of an antifuse Field Programmable Gate Array (FPGA) for data acquisition, processing, and storage, as well as the power supply control, self-test, status monitor, and communication. Two bipolar

Table 1 Main parameters of the LEIS spectrometer

Main parameters	Present	Previous [25]
Ion energy range	50 eV–25 keV	100 eV–15 keV
Energy resolution ($\Delta E/E$)	8.5%	⩽13%
Analyzer constant K	8.9	~5.8
Field of view (azimuth×elevation angles)	360°×90° (−45°–45°)	360°×90° (−45°–45°)
Angular resolution (azimuth×elevation angles)	~5.5°×3°	⩽22.5°×8°
Geometric factor (for each channel)	~1.6×10^{-4} cm^2 sr eV/eV[a)]	~1.0×10^{-3} cm^2 sr eV/eV[a)]

a) Considering the MCP efficiency and the grid transmittance.

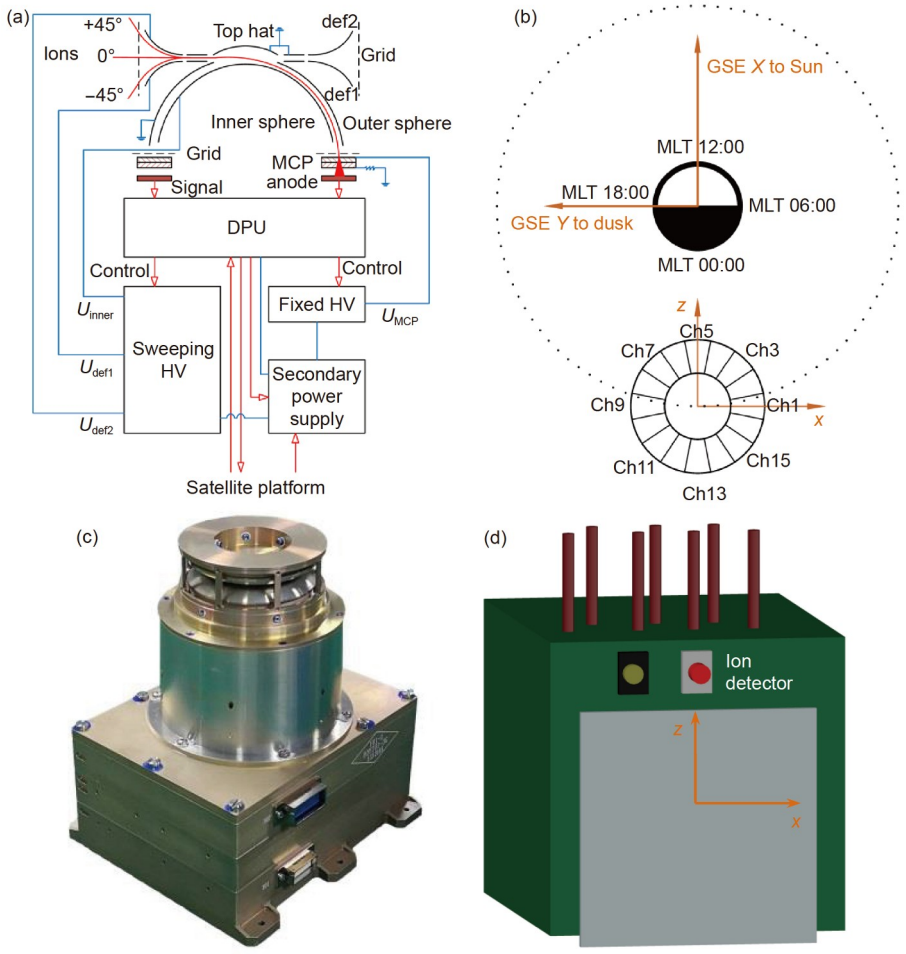

Figure 1 (a) Structural and functional schematic diagram of the LEIS spectrometer; (b) the payload photograph; (c) the diagrammatic sketch of flying along the GEO orbit around the Earth; (d) the location of payload on the spacecraft.

sweeping HV power supplies (−3 to +3 kV), one unipolar negative HV power supply (0 to −3 kV), and an adjustable negative HV power supply (0 to −3 kV) are integrated into an HV board, which are applied to a pair of the entrance deflectors, the inner sphere and the MCP electrodes, respectively. The sweeping steps of HV supplies and the stay time at each of the steps can be arranged via RS422 instructions. The required low voltages of the DPU and HV supplies are obtained through the conversion of a primary power supply from the satellite platform to a secondary power supply board.

The LEIS payload is produced via the integration of a sensor head and an electronic box as displayed in Figure 1(b). The sensor head includes the entrance deflectors, the ESA, and the PSD while the electronic box has three circuit boards, i.e., a DPU board, an HV board, and a secondary power supply board. The GEO satellite is a three-axis stabilized spacecraft that keeps one of its spacecraft axes (+z panel) facing the Earth and the +x panel towards its flight direction, as Figure 1(c) and (d) illustrated, the LEIS payload located in

the $-y$ panel of the spacecraft. The Ch1 is towards the moving direction of the spacecraft and the Ch5 always points to the Earth.

After the satellite launching, the LEIS payload was required to fulfill degassing at a suitable period of time. Subsequently, within the permitted time, the inflight tests have been carried out including self-checking of electronics, communication with ground station each other, HV scanning and controlling, adjustment and optimization of amplifier thresholds and MCP voltages, and storage and transmission of the data, etc. The normal measurements for the scientific data collection started on Sep 24, 2021. In the inflight measurement, the voltages of U_{inner} (0 to −2900 V), U_{def1} and U_{def2} (−2800 V to +2800 V) are swept synchronously with an exponential change, as Figure 2(a) and (b) illustrated, keeping a fixed ratio of ESA and deflector voltages to maintain a constant viewing elevation angle. There are 64 basic energy bins with 8.5% increment step by step for the coverage of ion energies from 50 eV/q up to 25 keV/q, and 15 angular bins for the elevation angles from −45° to 45°. Each elevation angle takes 128 steps as a minor cycle including 64 upward and 64 downward sweeping steps. In the last cycle, all voltages are set to zero for recording the possible UV light response and background noise. In the above work mode, energetic ions around the GEO orbit can be measured with a large FOV of 360°×90º and a wide energy range of 50 eV–25 keV per charge by using the simultaneous detections of 16 channels. Here, as a representative, the initial data measured by Ch5 and Ch13 on a day of Sep 30, 2021 (universal time, UT) are presented in Figure 2(c) and (d). One can see that three-dimensional measurements of energetic ions in space with the 360°×90° FOV and up to 25 keV/q energy range have been achieved. Note that due to the shielding of the spacecraft itself as shown in Figure 1(d), ions from some certain elevation angles cannot be detected by several channels, e.g., Ch13. This defect can be avoided by selecting the installation location in the future.

From the initial data measured inflight at the specific times, the energies and fluxes distributions of ions in temporal and spatial contexts have been obtained according to the instrumental parameters determined in the laboratory. The energy of detected ions is determined by the product of the analyzer constant (K=8.9) and the ESA voltage U_{inner}. The differential energy flux of ions is achieved via the quotient of the measured counts and the geometric factor (GF= 1.6×10^{-4} cm^2 sr eV/eV, considering the MCP efficiency of 50% and the grid transmittance of 81%). Taking into account the fact that the signals from the LEIS sensor might be contaminated by the background noises and solar UV light response occasionally, the data from such false signals have been deducted in order to obtain the true ion data. The amount of background noise and possible UV contamination can be determined by the counts recorded in the last cycle

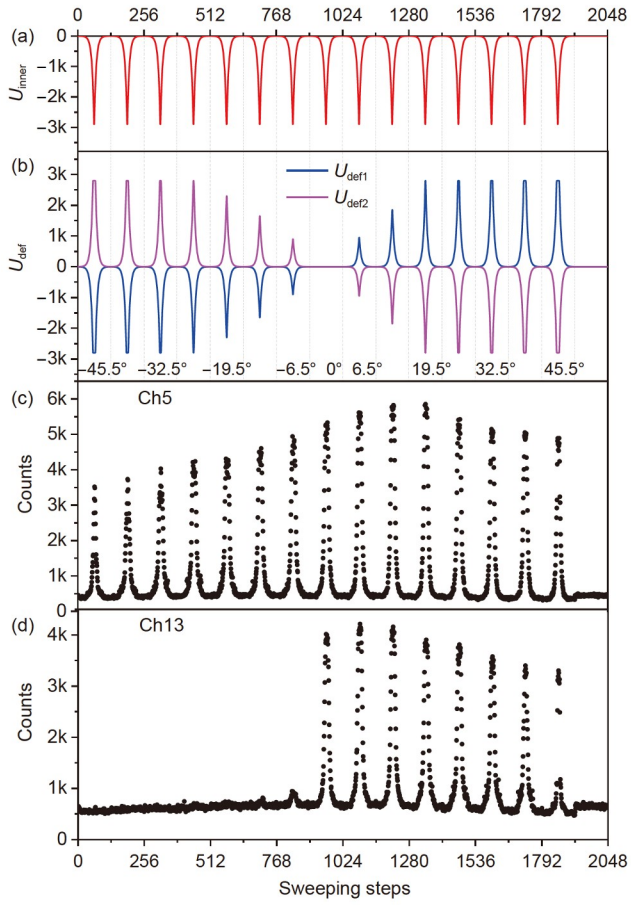

Figure 2 Sweeping voltages with an exponential step for (a) the inner sphere U_{inner} and (b) the entrance deflectors U_{def1} and U_{def2}. The initial data of inflight measurements on Sep 30, 2021, for the specific azimuthal angle channels (c) Ch5 and (d) Ch13, respectively.

time where the voltages of U_{inner}, U_{def1} and U_{def2} are all set to zero as Figure 2 shown. Figure 3 presented the ion energy and flux results for the representative Ch5 and Ch13 measured at the UT time from 2021-09-30/04:29 to 2021-10-01/04:29 corresponding to one magnetic local time (MLT) 12:00 and the next adjacent MLT 12:00. Since the satellite position varies continually in a day, the time of each channel facing the Sun is different. As a result, the strong UV response for different channels emerged at different times. For Ch5 and Ch13, as Figure 3(b) and (e) shown, the strong UV response for Ch5 mainly appeared near the MLT 00:00, several hours before and after it, while that for Ch13 mostly appeared around the MLT 12:00, that is, at this time Ch13 toward the Sun. As the figure displayed, although the UV response is noticeable because the LEIS sensor is exposed to solar UV lights occasionally, the remarkable enhancements of ion fluxes emerge at the specific energy region (e.g., ~1 keV or above 10 keV) and a certain time of a day, which suggests the occurrence of surface charging or substorm events. Further analysis will be presented in the next section.

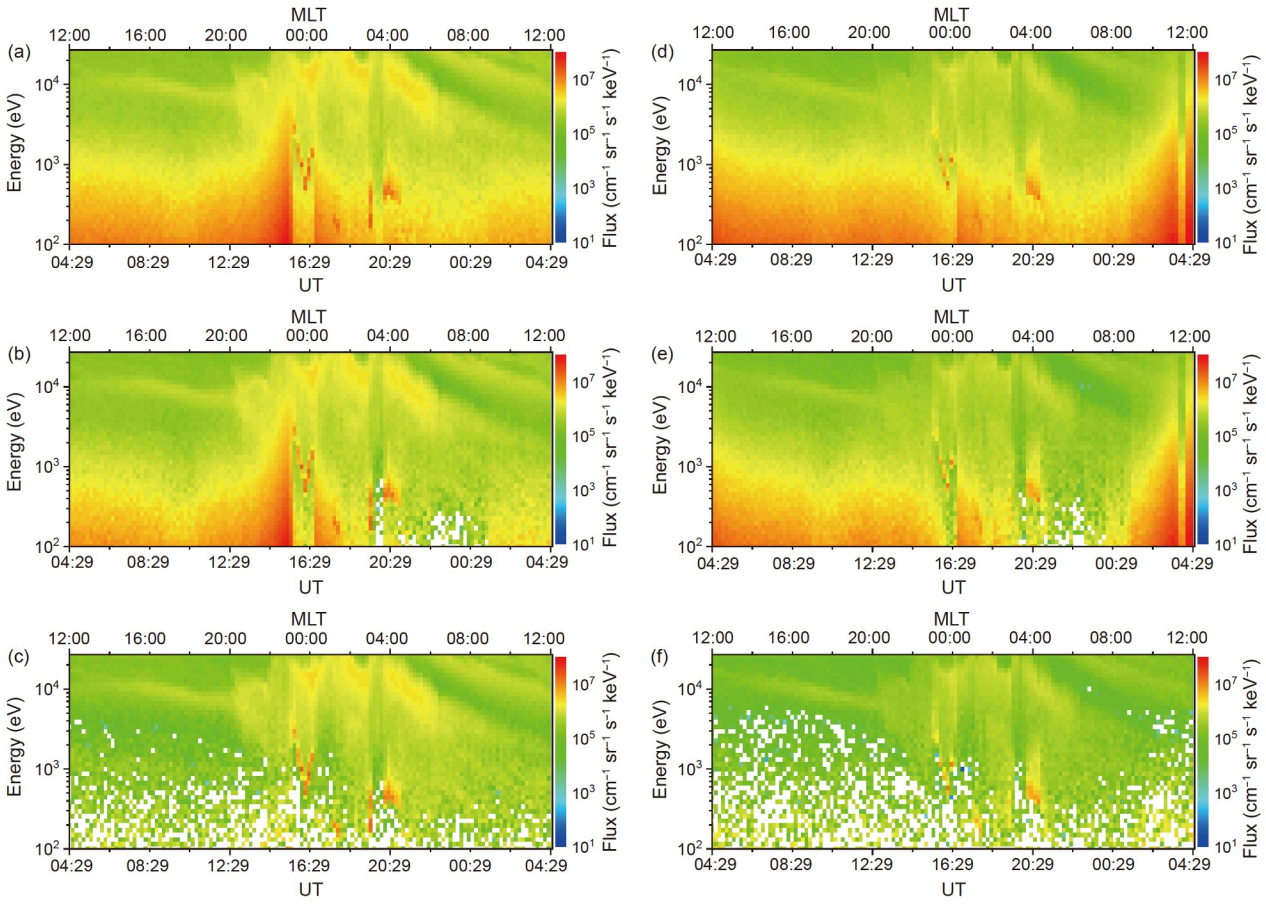

Figure 3 Differential energy flux spectra of ions measured on a day of Sep 30, 2021. (a)–(c) for Ch5; (d)–(f) for Ch13. The top panels are the initial data. The middle panels are the data with background noise subtracted. The bottom panels are the data with UV response further deducted.

3 Results and discussion of initial observations

Figure 4 presents the quantitative differential energy flux data measured in three months from Sep 24 to Dec 31, 2021, together with the available data from the Van Allen Probes mission [15,16] for comparison. Although their orbits are low inclining and highly elliptical (perigees ~0.1R_E, apogees ~6R_E, and periods ~9 h), different from the geosynchronous orbit, they do frequently cross the L shell of 6.6 near the equatorial plane. One can see from the figure that the present flux data from Ch1 (minimum flux), Ch10 (maximum flux) and the average of all 16 channels locate between the lower and upper boundary of the proton flux from the Van Allen Probes mission, close to their mean values, illustrating the reliability of the present measurement. These *in situ* measurement data could be applied to estimate the distribution of ring current ions, analyze the associated wave instabilities and understand complex dynamics of the outer radiation belt.

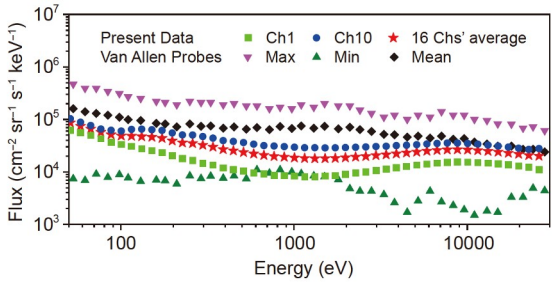

Figure 4 Differential energy flux of ions measured in three months from 2021-09-24 to 2021-12-31, together with the data from the Van Allen Probes near L=6.6 during 2013–2015.

Figure 5 shows the evolution of daily-averaged energetic ion fluxes during three months. The geomagnetic index *Sym*/*H* (daily-averaged data from the OMNIWeb) is also plotted in the figure. The *Sym*/*H* is essentially the same as the *Dst* index, and is usually applied to quantify the level of magnetic storms. One can see from the figure that the *Sym*/*H* index can decrease to over −30 nT, even −65 nT (peak value) in October and November, which represents the occurrence of small or moderate storms during this period according to the classification of geomagnetic storms [26,27]. A larger negative *Sym*/*H* means a more intense storm, and generally a more intense magnetospheric ring current due to the energetic particle ejections associated with the storm activities. The noticeable flux enhancements of ions with energies above 2 keV are observed clearly, indicating the signature of storm occurrences. The local increase of ion fluxes in the low

energy region of hundreds of eV is the result of spacecraft surface charging. A detailed discussion will be presented in the next part. It is noted that during the storms (e.g., October 17–19) the ion fluxes can reach 2×10^6 cm^{-2} sr^{-1} s^{-1} keV^{-1}, larger order of magnitude than those observed during the relatively quiescent times (e.g., October 22–25).

Figure 6 gives a zoom-in view of ion evolution driven by geomagnetic storms and substorms from 2021-10-17/04:29 UT, corresponding to MLT12:00, to 2021-10-21/04:29. As a comparison, the solar wind speed, the southward interplanetary magnetic field (IMF), the geomagnetic H component (*Sym*/*H* index) and the SME index are also plotted in Figure 6(b) and (c). One can see from Figure 6(c) that the

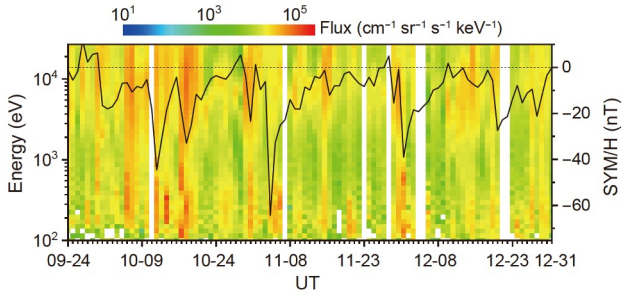

Figure 5 Daily averaged differential energy flux of ions measured by Ch5 from 2021-09-24 to 2021-12-31, and the daily-averaged SYM/H index from the NASA OMNIWeb.

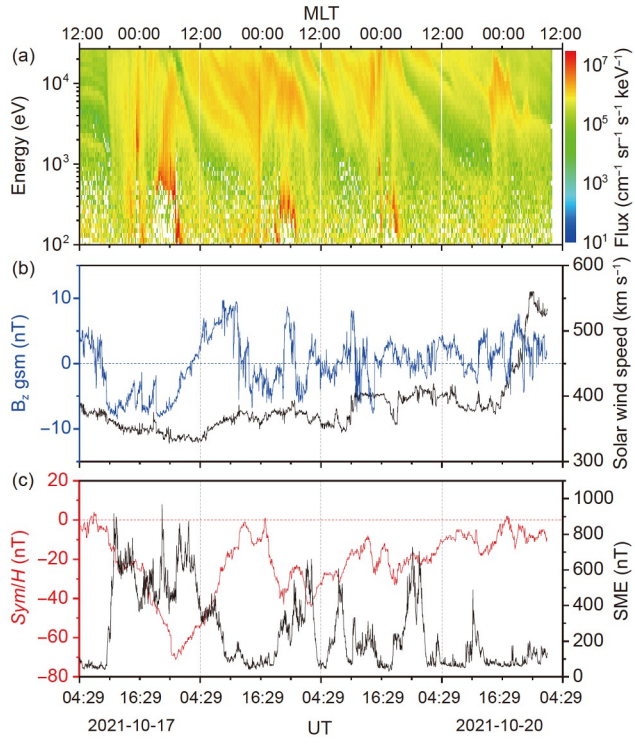

Figure 6 (a) Differential energy flux spectra of ions measured by Ch5 in four days from 2021-10-17 to 2021-10-20; (b) solar wind speed and B_Z gsm; (c) *Sym*/*H* and SME indexes. The data in (b) and (c) are obtained from the NASA OMNIWeb, World Data Center at Kyoto, and SuperMAG, respectively.

sudden slight increase of the *Sym*/*H* index at about 07:00 UT on 2021-10-17 reveals the sudden storm commencement (SSC) that signals the arrival of the geomagnetic storm (the initial phase). Immediately a significant *Sym*/*H* drop arises, slowly down to −70 nT at about 23:00 UT (the main phase). Then it returns gradually to normal condition (the recovery phase) at about 15:00 UT on 2021-10-18. Such an evolution behavior of the *Sym*/*H* index shows the characteristic signature of a moderate storm. Subsequently, a small storm also occurs and persists for about 24 h from 16:29 of Oct 18 to 16:29 of Oct 19, 2021. As shown in Figure 6(c), the slow solar wind speed suggests a typical Coronal mass ejection (CME) or Corotating Interaction Region (CIR) events are unlikely. While the southward interplanetary magnetic field (IMF), which occurred during *Sym*/*H* initial phase and main phase during the first 24-h timespan, may play a major role in trigging the occurrence of these magnetic storms. As a result, as shown in Figure 6(a), the storm/substorm-induced ion injections are recorded by the energy-dispersive wedge-like structures at energies above 2 keV, and the surface charging events are also signified by the bright line structures at energies of hundreds or thousands of eV.

The surface charging in the dawn sector may be caused by bulk hot plasma injection at the substorm [6]. During the southward IMF period, the dayside reconnection and magnetotail reconnection might be the major source of injecting intensive plasma flux to the geosynchronous orbit. The intensive plasma injection may cause strong satellite surface charging at dawn side of the geosynchronous orbit. Such plasma injections roughly coincided with the decrease in *Sym*/*H*. Three obvious illustrations of possible surface charging characteristics are shown in Figure 6(a). The lower limit of ions energy of the surface charging feature is around 560 eV. As a result, the accumulation effect appeared, leading to the intensity enhancement in the energy spectra of ions detected. Therefore, the charging potential on the spacecraft surface can be deduced on the basis of the sudden enhancement of ion fluxes. Because the major ions of plasma are protons, the surface charging potential of the first 24-h timespan was around 560 V. In the next two 24-h timespans, surface charging potentials became lower gradually. In the last 24-h timespan, the surface charging feature disappeared. Both charging potential and ion flux were enhanced in the main phase of the geomagnetic storm. Magnetometer station measurement, SME data from superMAG, also presented gradually weakened surges to coincide with surface charging events, because the southward IMF frequently appeared during the recovery phase and caused a saw-like *Sym*/*H* and SME profile.

4 Conclusion and expectation

The first results of a low-energy ion spectrometer payload

onboard the Chinese GEO satellite are presented. Three-dimensional measurements of energetic ions in space with a large field of view of 360°×90° and a wide energy range from 50 eV to 25 keV per charge have been achieved, and the differential energy flux spectra of the ions around the GEO orbit have been obtained in 90 days from 2021-09-24 to 2021-12-31. The remarkable local enhancements of ion fluxes in the energy region of above 2 keV or hundreds of eV are observed clearly, revealing the ion-ejection signatures from the notable storm/substorm or the associated surface charging that occurred during this period as the *Sym*/*H* index revealed. The occurrence of surface charging could be ascribed to the lack of photoemission at the Earth's eclipse (near midnight) or the ion injection at the dawn sector induced by geomagnetism storm/substorms. The present results demonstrated a good performance of the LEIS payload in flight as monitoring the space ion environment around the orbit. Meanwhile, it also indicated that the *in situ* measurement of space ions utilizing the LEIS can provide us an opportunity to study spacecraft charging and storm/substorms, as well as to understand the magnetospheric ion dynamics. As for space weather forecasting applications, further work will focus on searching for the link between some electric circuit anomaly and surface charging of the spacecraft. More data analysis, associated with the observations of other payloads for the plasma monitor onboard the satellite, is essentially needed.

This work was supported by the grants from Chinese Academy of Sciences (Grant Nos. XDB41000000, QYZDB-SSW-DQC015), and the National Natural Science Foundation of China (Grant No. 42188101). The authors would like to thank all the collaborators from the Shandong Institute of Space Electronic Technology and China Academy of Space Technology for their help in the fabrication and environmental tests of this payload.

1 Ishii M, Shiota D, Tao C, et al. Space weather benchmarks on Japanese society. Earth Planets Space, 2021, 73: 108
2 Katz S, Goldvais U, Price C. The connection between space weather and single event upsets in polar low earth orbit satellites. Adv Space Res, 2021, 67: 3237–3249
3 Ferguson D C, Worden S P, Hastings D E. The space weather threat to situational awareness, communications, and positioning systems. IEEE Trans Plasma Sci, 2015, 43: 3086–3098
4 Thomsen M F, Henderson M G, Jordanova V K. Statistical properties of the surface-charging environment at geosynchronous orbit. Space Weather, 2013, 11: 237–244
5 Ganushkina N Y, Swiger B, Dubyagin S, et al. Worst-case severe environments for surface charging observed at LANL satellites as dependent on solar wind and geomagnetic conditions. Space Weather, 2021, 19: e02732
6 Spence H E, Blake J B, Fennell J F. Surface charging analysis of high-inclination, high-altitude spacecraft: Identification and physics of the plasma source region. IEEE Trans Nucl Sci, 1993, 40: 1521–1524
7 Nicolaou G, Wicks R T, Rae I J, et al. Evaluating the performance of a plasma analyzer for a space weather monitor mission concept. Space Weather, 2020, 18: e2020SW002559
8 Lin R P, Anderson K A, Ashford S, et al. A three-dimensional plasma and energetic particle investigation for the wind spacecraft. Space Sci Rev, 1995, 71: 125–153
9 Barabash S, Sauvaud J A, Gunell H, et al. The analyser of space plasmas and energetic atoms (ASPERA-4) for the venus express mission. Planet Space Sci, 2007, 55: 1772–1792
10 Rème H, Bosqued J M, Sauvaud J A, et al. The cluster ion spectrometry (CIS) experiment. Space Sci Rev, 1997, 79: 303–350
11 Rème H, Aoustin C, Bosqued J M, et al. First multispacecraft ion measurements in and near the Earth's magnetosphere with the identical Cluster ion spectrometry (CIS) experiment. Ann Geophys, 2001, 19: 1303–1354
12 Carlson C W, McFadden J P, Turin P, et al. The electron and ion plasma experiment for FAST. Space Sci Rev, 2001, 98: 33–66
13 Young D T, Berthelier J J, Blanc M, et al. Cassini plasma spectrometer investigation. Space Sci Rev, 2004, 114: 1–112
14 Barabash S, Lundin R, Andersson H, et al. The analyzer of space plasmas and energetic atoms (Aspera-3) for the Mars Express Mission. Space Sci Rev, 2006, 126: 113–164
15 Funsten H O, Skoug R M, Guthrie A A, et al. Helium, Oxygen, Proton, and Electron (HOPE) mass spectrometer for the radiation belt storm probes mission. Space Sci Rev, 2013, 179: 423–484
16 Spence H E, Reeves G D, Baker D N, et al. Science goals and overview of the radiation belt storm probes (RBSP) energetic particle, composition, and thermal plasma (ECT) suite on NASA's Van Allen probes mission. Space Sci Rev, 2013, 179: 311–336
17 Saito Y, Yokota S, Asamura K, et al. In-flight performance and initial results of plasma energy angle and composition experiment (PACE) on SELENE (Kaguya). Space Sci Rev, 2010, 154: 265–303
18 Kong L G, Wang S J, Wang X Y, et al. In-flight performance and preliminary observational results of Solar Wind Ion Detectors (SWIDs) on Chang'E-1. Planet Space Sci, 2012, 62: 23–30
19 Zou H, Ye Y G, Zong Q G, et al. Imaging energetic electron spectrometer onboard a Chinese navigation satellite in the inclined GEO orbit. Sci China Tech Sci, 2018, 61: 1845–1865
20 Halekas J S, Taylor E R, Dalton G, et al. The solar wind ion analyzer for MAVEN. Space Sci Rev, 2015, 195: 125–151
21 McFadden J P, Kortmann O, Curtis D, et al. MAVEN SupraThermal and Thermal Ion Compostion (STATIC) instrument. Space Sci Rev, 2015, 195: 199–256
22 Pollock C, Moore T, Jacques A, et al. Fast plasma investigation for magnetospheric multiscale. Space Sci Rev, 2016, 199: 331–406
23 Kong L G, Zhang A B, Tian Z, et al. Mars Ion and Neutral Particle Analyzer (MINPA) for Chinese Mars Exploration Mission (Tianwen-1): Design and ground calibration. Earth Planet Phys, 2020, 4: 333–344
24 Liu K, Hao X J, Li Y R, et al. Mars orbiter magnetometer of China's First Mars Mission Tianwen-1. Earth Planet Phys, 2020, 4: 384–389
25 Hu R X, Shan X, Yuan G Y, et al. A low-energy ion spectrometer with half-space entrance for three-axis stabilized spacecraft. Sci China Tech Sci, 2019, 62: 1015–1027
26 Gonzalez W D, Joselyn J A, Kamide Y, et al. What is a geomagnetic storm? J Geophys Res, 1994, 99: 5771–5792
27 Vieira L E A, Gonzalez W D, Clua de Gonzalez A L, et al. A study of magnetic storms development in two or more steps and its association with the polarity of magnetic clouds. J Atmos Sol-Terrestrial Phys, 2001, 63: 457–461